PCCP

Accepted Manuscript

This is an *Accepted Manuscript*, which has been through the Royal Society of Chemistry peer review process and has been accepted for publication.

Accepted Manuscripts are published online shortly after acceptance, before technical editing, formatting and proof reading. Using this free service, authors can make their results available to the community, in citable form, before we publish the edited article. We will replace this *Accepted Manuscript* with the edited and formatted *Advance Article* as soon as it is available.

You can find more information about *Accepted Manuscripts* in the **Information for Authors**.

Please note that technical editing may introduce minor changes to the text and/or graphics, which may alter content. The journal's standard **Terms & Conditions** and the **Ethical guidelines** still apply. In no event shall the Royal Society of Chemistry be held responsible for any errors or omissions in this *Accepted Manuscript* or any consequences arising from the use of any information it contains.

Physical Chemistry Chemical Physics

Order and disorder in quaternary atomic laminates from first-principles calculations

Martin Dahlqvist* and Johanna Rosen

We report on the phase stability of chemically ordered and disordered quaternary MAX phases – TiMAlC, TiM_2AlC$_2$, MTi$_2$AlC$_2$, and Ti$_2M_2$AlC$_3$ where M=Zr,Hf (group IV), M=V,Nb,Ta (group V), and M=Cr,Mo,W (group VI). At 0 K, layered chemically ordered structures are predicted to be stable for M from group V and VI. By taking into account the configurational entropy, an order-disorder temperature $T_{disorder}$ can be estimated. TiM_2AlC$_2$ (M=Cr,Mo,W) and Ti$_2M_2$AlC$_3$ (M=Mo,W) are found with $T_{disorder}$ >1773 K and are hence predicted to be ordered at the typical bulk synthesis temperatures of 1773 K. Other ordered phases, even though metastable at elevated temperatures, may be synthesized by non-equilibrium methods such as thin film growth. Furthermore, phases predicted not to be stable in any form at 0 K can be stabilized at higher temperatures in a disordered form, being the case for group IV, for MTi$_2$AlC$_2$ (M=V,Cr,Mo), and for Ti$_2M_2$AlC$_3$ (M=V,Ta). The stability of the layered ordered structures with M from group VI can primarily be explained by Ti breaking the energetically unfavorable stacking of M and C where M is surrounded by C in a face-centered cubic configuration, and by M having a larger electronegativity than Al resulting in fewer electrons available for populating antibonding Al-Al orbitals. The results show that these chemically ordered quaternary MAX phases allow for new elemental combinations in MAX phases, which can be used to add new properties to this family of atomic laminates and in turn prospects for tuning these properties.

1 Introduction

Atomic laminates with the general formula $M_{n+1}AX_n$ (n = 1 - 3), where M is an early transition metal, A is a group 13 to 16 element, and X is carbon and/or nitrogen, have attracted interest due to their combination of attributes from metals and ceramics such as good machinability, electrical and thermal conduction, heat and oxidation resistance, damage tolerance, and a maintained strength at high temperatures. [1, 2] Recently also magnetism was been added to the long list of attainable properties for these so-called MAX phases.[3, 4]

To date ~70 ternary MAX phases have been synthesized with Nb$_2$GeC[5] and Mn$_2$GaC[6, 7] being among the latest additions to this family of compounds. Adding a fourth element by alloying on the M- A- and/or X site allows for even more elemental combinations. In particular, solid solutions on the M-site include, e.g., (Ti,M)$_2$AlC where M = V, Nb, Ta, Cr,[8-11] (V,M)$_2$AlC where M = Nb, Ta, Cr,[9, 12] (Cr,Mn)$_2$$A$C where A = Al, Ga, Ge,[3, 13-19] (Ti,V)$_3$$AC_2$ where A = Al, Ge,[20, 21] and (V,M)$_4$AlC$_3$ where M = Ti, Nb.[20, 21] Adding a fourth element has also been demonstrated by realization of TiCr$_2$AlC$_2$,[22, 23] V$_{1.5}$Cr$_{1.5}$AlC$_2$,[12] TiMo$_2$AlC$_2$,[24, 25] and Ti$_2$Mo$_2$AlC$_3$,[24] which all are recent discoveries of *chemically ordered* quaternary MAX phases, with atomic layers composed of a single element only. This raises the question why certain combinations of M elements form layered chemically ordered MAX phases, while other combinations result in a solid solution. In both cases, new alloys may allow incorporation of elements beside those included to date which, in turn, may enable addition of new properties and prospects for tuning these properties. Furthermore, novel MAX phase alloys may allow realization of new 2D counterparts, so called MXenes,[26] from chemical etching of the A-layer.

In this work, we have performed first-principles calculations on (Ti,M)$_{n+1}$AlC$_n$ phases (n = 1 - 3), to explore chemically ordered and disordered distributions of Ti and M on the M-site for M = Zr, Hf, V, Nb, Ta, Cr, Mo, W. This allows a systematic investigation with M elements spanning over group IV, V, and VI and period 4, 5, and 6 in the periodic table of elements. A is kept equal to Al, since i) all chemically ordered MAX phase alloys reported to date include A = Al,[12, 22-25] i.e. this choice allows theoretical validation of previous experimental results as well as prediction of new alloys, and ii) to date, all known MXenes[26] originate from chemical etching of Al from a MAX phase,[26] with the only exception of Mo$_2$C,[27] i.e. here predicted new alloys implies potentially new MXenes. Recently, chemically ordered MXenes were produced from chemically ordered quaternary MAX phases.[28]

This study is divided into two parts. In the first part, we perform explanatory and predictive calculations with respect to stability of chemically ordered as well as disordered quaternary MAX phases. The calculations confirm the stability of the quaternary phases reported to date, and also suggest several ordered as well as disordered novel alloys. In the second part,

Thin Film Physics Division, Department of Physics, Chemistry and Biology (IFM), Linköping University, SE-581 83 Linköping, Sweden. E-mail: martin.dahlqvist@liu.se

the driving force behind the formation of the layered chemically ordered MAX phases is discussed in terms of atomic stacking sequences of M and C, electronegativity of M and Al, and the electronic structure and chemical bonding between the constituting elements.

2 Computational Methods

First-principles calculations were performed by means of density functional theory (DFT) and the projector augmented wave method[29, 30] as implemented within the Vienna *ab-initio* simulation package (VASP).[31-33] We adopted the generalized gradient approximation (GGA) as parameterized by Perdew-Burke-Ernzerhof (PBE)[34] for treating electron exchange and correlation effects. A plane-wave energy cut-off of 400 eV was used and for sampling of the Brillouin zone we used the Monkhorst-Pack scheme.[35] For each considered phase the calculated total energy is converged to within 0.5 meV/atom with respect to k-point sampling and structurally optimized in terms of unit-cell volumes, c/a ratios (when necessary), and internal parameters to minimize the total energy.

For all $(Ti, M)_{n+1}AlC_n$ compositions, we considered different layered chemically ordered structures, *hereafter referred to as just ordered structures*, defined in Fig. 1 for $n = 1$ with Ti:M = 1:1 (type A, B, C, D), $n = 2$ with Ti:M = 2:1 and 1:2 (type A, B, C, D, E, F), and $n = 3$ with Ti:M = 2:2 composition (type A, B). Spin-polarization have been considered for Cr-based phases in the form of non-magnetic (NM), ferromagnetic (FM) and up to five different antiferromagnetic (AFM) spin configurations for each ordered structure. Detailed information of these spin configurations are given in Table S1 to S10.

Chemically disordered structures, *hereafter referred to as just disordered structures*, denote a solid solution of M and Ti on the M-sites. These are modelled using the special quasi-random structure (SQS) method[36, 37] on supercells of $4\times4\times1$ M_2AX, M_3AX_2, and M_4AX_3 unit cells, with a total of 64, 96, and 128 M-sites, respectively. Convergence tests with respect to

total energy show that these sizes are appropriate to use, based on an energy of the $4\times4\times1$ unit cells being within 2 meV/atom compared to larger supercells.

For a MAX phase to be thermodynamically stable its energy $E(MAX)$ should be lower than the energy of any linear combination of all other competing phases in the system which corresponds to the MAX phase stoichiometry, i.e.,

$$\Delta H_{cp} = E(MAX) - E(\text{competing phases}) < 0, \qquad (1)$$

where ΔH_{cp} is the formation enthalpy. In order to identify the set of most competing phases at a given composition we make use of a linear optimization procedure[37, 38] which have been proven successful to confirm already experimentally known MAX phases as well as predicting the existence of new ones.[3, 5, 6, 14, 38, 39]

When the temperature $T \neq 0$ K, Gibbs free energy of a disordered phase, $\Delta G_{cp}^{disorder}$, can be approximated using

$$\Delta G_{cp}^{disorder} = \Delta H_{cp}^{disorder} - T\Delta S, \qquad (2)$$

where ΔS is the entropy per formula unit of an ideal solution of Ti and M atoms on the M-sites, expressed as

$$\Delta S = -yk_B\left[z\ln(z) + (1-z)\ln(1-z)\right], \qquad (3)$$

where y is number of M-sites per formula unit, i.e., $y = n + 1$, and $z = M/(M + Ti)$.

Chemical bonding was investigated in terms of projected crystal orbital Hamiltonian populations (pCOHP) which were derived using the LOBSTER program.[40-42] Using this method the calculated band-structure energy is reconstructed into orbital interactions. Positive pCOHP values indicate an anti-bonding interaction, and negative pCOHP values indicate a bonding interaction.
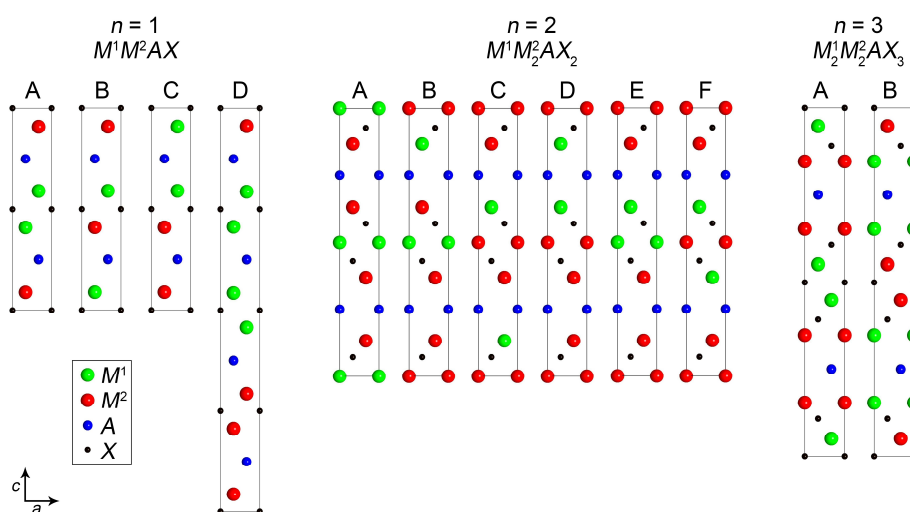
Fig. 1 Schematic illustration of ordered type structures considered for $(Ti, M)_{n+1}AlC_n$ where $n = 1 - 3$. These projections are viewed along the $[1\bar{2}10]$ direction.

Journal Name

3 Results and Discussion

3.1 Phase stability of known and hypothetical MAX phase alloys

The formation enthalpy ΔH_{cp} for ordered and disordered configurations of Ti and M on the M-site (ordered type structures as shown in Fig. 1) has been calculated for MTiAlC, TiM_2AlC$_2$, MTi$_2$AlC$_2$, and Ti$_2M_2$AlC$_3$ compositions. The results are listed in Table 1 to 4, respectively, along with the identified set of most competing phases (the last column of each table). For Cr-based phases, the spin configuration of lowest energy is presented and specified. For a systematic analysis including identification of trends, selected results are also displayed in Fig 2 to 4.

Throughout this section, the stability of ordered and disordered structures will be discussed. At 0 K, the structure with lowest energy is considered stable if $\Delta H_{\mathrm{cp}} < 0$. However, when $T \neq 0$ K, the configurational entropy ΔS will decrease the free energy for the solid solutions, $\Delta G_{\mathrm{cp}}^{\mathrm{disorder}}$. By using Eq. 2 and 3, an order-disorder temperature T_{disorder} can be calculated for which $\Delta G_{\mathrm{cp}}^{\mathrm{disorder}}[T] = \Delta H_{\mathrm{cp}}^{\mathrm{order}}$ is fulfilled, and hence give an estimate above which temperature the disordered structure is energetically favourable. This temperature can then be compared to experimental conditions used, e.g., typical bulk synthesis temperatures of 1200 - 1600 °C (1473 - 1873 K). We have chosen 1500 °C (1773 K) as a reference temperature for estimating preferred order or disorder in an alloy. Hence, for $\Delta H_{\mathrm{cp}}^{\mathrm{order}} < 0$ and $T_{\mathrm{disorder}} > 1773$ K, the ordered structure is predicted to be the most likely outcome in bulk synthesis. If $\Delta H_{\mathrm{cp}}^{\mathrm{order}} < 0$ and $T_{\mathrm{disorder}} < 1773$ K, a resulting disordered structure is suggested. However, it should be stressed that use of reduced synthesis temperature or techniques based on different synthesis kinetics, such as thin film growth, may allow realization of stable as well as metastable phases, i.e. ordered phases with low critical temperatures or even with ΔH_{cp} or $\Delta G_{\mathrm{cp}} > 0$.

TiMAlC

Figure 2 (based on Table I) shows the formation enthalpies ΔH_{cp} as function of M in TiMAlC for the ordered structure of lowest energy (black bars) and for a solid solution of Ti and M (red bars). Only M from group V are found to give $\Delta H_{\mathrm{cp}} < 0$, and these phases are hence predicted to be stable. The lowest energies are obtained for the ordered structures, however, at elevated temperatures the free energy for the solid solution, $\Delta G_{\mathrm{cp}}^{\mathrm{disorder}}$, may be reduced to values below ΔH_{cp}. The temperatures that fulfils $\Delta G_{\mathrm{cp}}^{\mathrm{disorder}}[T] = \Delta H_{\mathrm{cp}}^{\mathrm{order}}$ are plotted as open squares in Fig. 2. For all M, the temperature needed to fulfil this criteria is $T < 650$ K, which is significantly below 1773 K. A disordered distribution of Ti and M is therefore expected in material synthesis. The here predicted disordered and stable 211 MAX phase alloys including M = V, Nb, and Ta are consistent with reported bulk synthesis of (Ti$_{0.5}$V$_{0.5}$)$_2$AlC,[8, 9, 11, 43] (Ti$_{0.5}$Nb$_{0.5}$)$_2$AlC,[9, 10, 44] and (Ti$_{0.4}$Ta$_{0.6}$)$_2$AlC MAX phases,[9] all displaying solid solutions of M and Ti.

If $\Delta H_{\mathrm{cp}}^{\mathrm{order}} > \Delta H_{\mathrm{cp}}^{\mathrm{disorder}} > 0$, the order-disorder temperature becomes negative and hence unphysical. For such situation the temperature for which $\Delta G_{\mathrm{cp}}^{\mathrm{disorder}}[T] = 0$ is

Table 1 Calculated formation enthalpy ΔH_{cp} for TiMAlC where M = Zr, Hf, V, Nb, Ta, Cr, Mo, W, including ordered (type A to D, shown in Fig. 1, with M^A = Ti and M^B = M) and disordered (SQS) distribution of Ti and M on the M-site. The last column shows the identified set of most competing phases. See Table S1 to S4 for definition of considered spin configurations for TiCrAlC.

| M | ΔH_{cp} (meV/atom) | | | | | Identified set of most competing phases |
	A	B	C	D	SQS	
Zr	13	9	11	15	1	TiC, Zr$_4$Al$_3$, Zr$_3$Al$_3$
Hf	37	34	37	39	30	Hf$_3$AlC2, Ti$_2$AlC, TiAl
V	10	-2	5	15	2	Ti$_2$AlC, V$_2$AlC
Nb	5	-16	-18	9	-10	NbTi$_2$AlC$_2$ (D), Nb$_2$Al, NbAl$_3$
Ta	7	-23	-21	13	-17	TaTi$_2$AlC$_2$ (A), TiAl$_2$, Ta$_2$C
Cr	38[a]	16[b]	40[c]	34[d]	34[e]	TiC, Cr$_2$Al, TiAl$_3$, TiCr$_2$AlC$_2$ (A)
Mo	85	35	51	98	46	TiC, Mo$_3$Al, Mo$_3$Al$_8$
W	88	3	27	106	13	WTi$_2$AlC$_2$ (C), W, WAl$_5$

a NM spin configuration of lowest energy.
b in-AFM1 spin configuration of lowest energy.
c in-AFM2 spin configuration of lowest energy.
d in-AFM1 spin configuration of lowest energy.
e FM spin configuration of lowest energy.
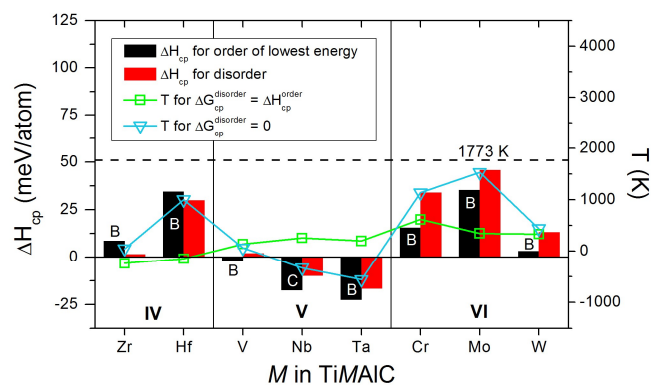
Fig. 2 Formation enthalpy ΔH_{cp} for MTiAlC, for the ordered structure of lowest energy (black bar) and the disordered structure (red bar), together with the estimated temperature for which the disordered structure is stabilized, $T_{\Delta G=0}$ (open triangles), and the temperature above which the disordered structure is energetically favourable compared to the ordered one, T_{disorder} (open squares). The dashed horizontal line represents a typical bulk synthesis temperature of 1773 K.

fulfilled, denoted $T_{\Delta G=0}$, is more relevant as it indicates above which temperature the disordered alloy becomes stable (i.e. with a negative formation free energy). This is shown as open triangles in Fig. 2. The disordered structure of both TiZrAlC and TiWAlC are found with positive, though close to zero, values of $\Delta H_{\mathrm{cp}}^{\mathrm{disorder}}$, +1 and +13 meV/atom, respectively. Hence, the disordered structures of these phases are in theory stabilized for temperatures above 49 and 441 K, respectively, and may therefore be possible to synthesize.

MTi$_2$AlC$_2$ and TiM$_2$AlC$_2$

Fig. 3(a) shows ΔH_{cp} for MTi$_2$AlC$_2$, for the layered ordered structures of lowest energy (black bars) and for a solid solution of Ti and M on the M-site (red bars), together with the estimated temperature above which the disordered structure is energetically favourable compared to the ordered one, T_{disorder}, and $T_{\Delta G=0}$ for which the disordered structure is stabilized. Corresponding information for TiM_2AlC$_2$ is plotted in panel (b).

ARTICLE

Journal Name

For MTi$_2$AlC$_2$, M = Nb, Ta, and W have $\Delta H_{cp}^{order} < 0$ for ordered structures, suggesting that these phases are stable. However, the configurational entropy will decrease the free energy for the solid solutions, and make the disordered MTi$_2$AlC$_2$ compositions for M = Nb, Ta, and W energetically favourable for temperatures below typical bulk synthesis temperature, i.e., $T_{disorder} < 1773$ K. It should be noted that even though $\Delta H_{cp}^{order} > 0$ for ZrTi$_2$AlC$_2$, HfTi$_2$AlC$_2$, VTi$_2$AlC$_2$, CrTi$_2$AlC$_2$, and MoTi$_2$AlC$_2$, these solid solutions may be realized for elevated temperatures through a stabilizing Gibbs free energy as is indicated by blue triangles with $T_{\Delta G=0} < 1637$ K, i.e. these phases are likely to be found experimentally. Although the stoichiometry is slightly off from VTi$_2$AlC$_2$, this prediction can be compared to the experimentally obtained (V$_{0.5}$Ti$_{0.5}$)$_3$AlC$_2$ solid solution.[21]

For TiM_2AlC$_2$ in Fig. 3(b), M from group V and VI are found with $H_{cp}^{order} < 0$, indicating stable ordered phases. Two regimes of $T_{disorder}$ is found where (i) M from group IV and V have $T_{disorder} < 900$ suggesting a preferred solid solution of Ti and M, and (ii) M from group VI have $T_{disorder} > 3600$ K, indicating that ordered structures are expected at typical synthesis temperatures. For Group VI, type A layering is of lowest energy. Experimental findings of TiCr$_2$AlC$_2$ [22, 23] and TiMo$_2$AlC$_2$ [24, 25] with identified structures of type A corroborates these theoretical predictions. The here predicted stable ordered TiW$_2$AlC$_2$ is yet to be experimentally verified. Furthermore, even though TiZr$_2$AlC$_2$ is found with $H_{cp}^{order} > 0$, the disordered structure is estimated to be stabilized above 1464 K.

Table 2 Calculated formation enthalpy ΔH_{cp} for MTi$_2$AlC$_2$ where M = Zr, Hf, V, Nb, Ta, Cr, Mo, W, including ordered (type A to F, shown in Fig. 1 with $M^1 = M$ and M^2 = Ti) and disordered (SQS) distribution of Ti and M on the M-site. The last column shows the identified set of most competing phases. See Table S5 to S6 for definition of considered spin configurations for CrTi$_2$AlC$_2$.

M	ΔH_{cp} (meV/atom)							Identified set of most competing phases
	A	B	C	D	E	F	SQS	
Zr	34	42	50	52	45	52	44	Ti$_3$AlC$_2$, Zr$_3$AlC$_2$
Hf	17	34	51	52	36	51	39	HfC, Ti$_2$AlC
V	26	14	3	6	22	7	11	Ti$_3$AlC$_2$, TiV$_2$AlC$_2$ (A)
Nb	3	-1	-1	-5	19	4	0	TiNb$_2$AlC$_2$ (A), Ti$_3$AlC$_2$
Ta	-30	-19	-5	-6	7	1	-15	TiTa$_2$AlC$_2$ (A), Ti$_3$AlC
Cr	111^a	62^b	6^c	13^d	82^e	14^f	45^g	TiC, Cr$_2$Al, TiAl$_3$, TiCr$_2$AlC$_2$ (A)
Mo	91	55	9	24	108	14	31	TiC, Mo$_3$Al, Mo$_3$Al$_8$
W	39	22	-8	14	84	-7	-5	Ti$_2$W$_2$AlC$_3$ (A), Ti$_3$AlC$_2$, W, WAl$_5$

^{a} in-AFM2 spin configuration of lowest energy (FM, AFM1, and in-AFM1 within 1 meV/atom).
^{b} FM spin configuration of lowest energy (AFM1, in-AFM1 and in-AFM2 within 1 meV/atom).
^{c} NM spin configuration of lowest energy (FM, AFM1, in-AFM1, and in-AFM2 within 1 meV/atom).
^{d} FM spin configuration of lowest energy.
^{e} AFM1 spin configuration of lowest energy.
^{f} FM spin configuration of lowest energy (NM, AFM1, in-AFM1, and in-AFM2 within 1 meV/atom).
^{g} FM spin configuration of lowest energy.

Table 3 Calculated formation enthalpy ΔH_{cp} for TiM_2AlC$_2$ where M = Zr, Hf, V, Nb, Ta, Cr, Mo, W, including ordered (type A to F, shown in Fig. 1 with M^1 = Ti and $M^2 = M$) and disordered (SQS) distribution of Ti and M on the M-site. The last column shows the identified set of most competing phases. See Table S7 to S8 for definition of considered spin configurations for TiCr$_2$AlC$_2$.

M	ΔH_{cp} (meV/atom)							Identified set of most competing phases
	A	B	C	D	E	F	SQS	
Zr	56	46	34	37	48	35	40	Zr$_3$AlC$_2$, Ti$_3$AlC$_2$
Hf	91	73	55	56	74	55	64	TiAl, Hf$_2$Al, HfAl$_2$, Ti$_4$AlC$_3$
V	-8	9	20	30	21	26	16	V$_2$AlC, Ti$_2$V$_2$AlC$_3$ (A)
Nb	-13	4	14	21	13	13	4	Ti$_2$Nb$_2$AlC$_3$ (A), Nb$_2$AlC
Ta	-7	1	1	11	12	-4	-7	TaTi$_2$AlC$_2$ (A), Ta$_{12}$Al$_3$C$_8$, (Ti$_{0.5}$Ta$_{0.5}$)C, TaAl$_3$
Cr	-3^a	66^b	141^c	139^d	79^e	135^f	98^g	TiC, Cr$_2$AlC
Mo	-18	72	159	167	116	154	102	Ti$_2$Mo$_2$AlC$_3$ (A), Mo$_3$Al, Mo$_3$Al$_8$, C
W	-3	81	161	174	156	171	108	Ti$_2$W$_2$AlC$_3$ (A), WC, W, WAl$_5$

^{a} in-AFM1 spin configuration of lowest energy.
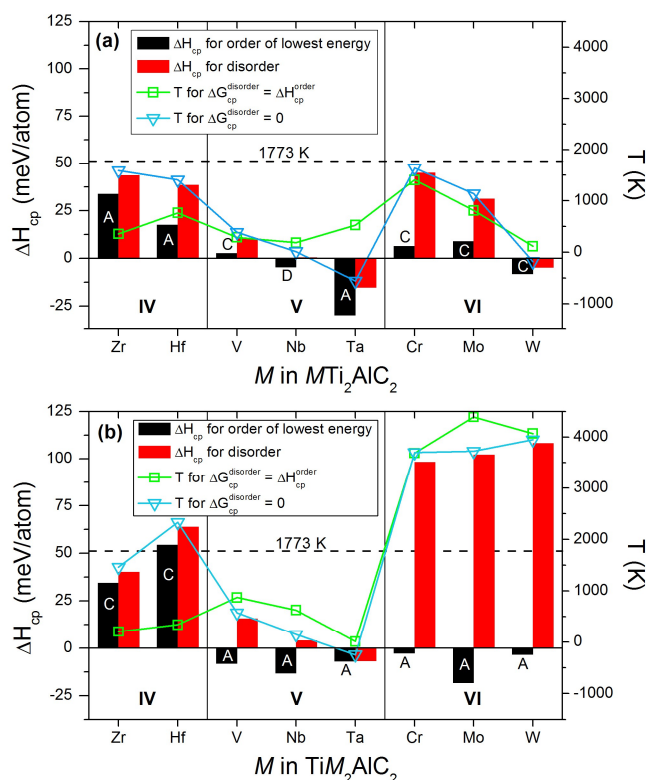^{b} FM spin configuration of lowest energy.
^{c} AFM3 spin configuration of lowest energy (FM and AFM1 within 1 meV/atom).
^{d} FM spin configuration of lowest energy.
^{e} AFM2 and AFM3 spin configuration degenerate and of lowest energy (FM within 1 meV/atom).
^{f} AFM1 spin configuration of lowest energy (FM within 1 meV/atom).
^{g} FM spin configuration of lowest energy.

Fig.3 Formation enthalpy ΔH_{cp} for (a) MTi$_2$AlC$_2$ and (b) TiM_2AlC$_2$, for the ordered structure of lowest energy (black bar) and the disordered structure (red bar), together with the estimated temperature for which the disordered structure is stabilized, $T_{\Delta G=0}$ (open triangles), and the temperature above which the disordered structure is energetically favourable compared to the ordered one, $T_{disorder}$ (open squares). The dashed horizontal line represents a typical bulk synthesis temperature of 1773 K.

Ti₂M₂AlC₃

Fig. 4 shows ΔH_{cp} for Ti₂M₂AlC₃, for the layered ordered structures of lowest energy (black bars) and for a disordered structure (red bars). $T_{disorder}$ is plotted as open squares, showing the estimated temperature above which the disordered structure is energetically favourable compared to the ordered one. For M = Nb, Mo, and W, stable ordered phases are indicated with $\Delta H_{cp}^{order} < 0$. However, for M = Nb, $T_{disorder}$ is well below 1773 K, i.e., a disordered structure is expected for typical synthesis conditions. As $T_{disorder} \geq 1870$ K for M = Mo, and W, ordered structures with A type layering are expected experimentally. Furthermore, it should be noted that $\Delta H_{cp}^{order} > 0$ but small for M = V, Ta, and Cr (+2, +12, and +3 meV/atom, respectively). Hence, for at least V and Ta, the configurational entropy may decrease the free energy for the solid solutions, and make the disordered Ti₂M₂AlC₃ energetically favourable and likely to be realized during synthesis.

Bulk synthesis of Ti₂Mo₂AlC₃ has shown structures where the Wyckoff 4f-site is mainly occupied by Ti and Wyckoff 4e-site mainly by Mo,[24] which is a configuration closely related to the fully ordered type A structure considered in this work. The predicted stable ordered Ti₂W₂AlC₂ and close to stable ordered Ti₂Cr₂AlC₃ of type A have not yet been identified experimentally.

Table 4 Calculated formation enthalpy ΔH_{cp} for Ti₂M₂AlC₃ where M = Zr, Hf, V, Nb, Ta, Cr, Mo, W, including ordered (type A and B, shown in Fig. 1 with M^1 = Ti and M^2 = M) and disordered (SQS) distribution of Ti and M on the M-site. The last column shows the identified set of most competing phases. See Table S9 to S10 for definition of considered spin configurations for Ti₂Cr₂AlC₃.

M	ΔH_{cp} (meV/atom)			Identified set of most competing phases
	A	B	SQS	
Zr	74	44	60	ZrC, Ti₃AlC₂, Zr₄AlC₃
Hf	84	27	55	HfC, Ti₂AlC
V	2	85	37	TiC, TiV₂AlC₂
Nb	-5	56	17	TiNb₂AlC₂ (A), TiC
Ta	12	17	4	(Ti₀.₅Ta₀.₅)C, TaTi₂AlC₂ (A), TiTa₂AlC₂ (A)
Cr	3[a]	203[b]	101[c]	TiC, Cr₂AlC
Mo	-17	173	71	TiC, TiMo₂AlC₂ (A)
W	-16	134	40	TiW₂AlC₂ (A), TiC

[a] in-AFM1 spin configuration of lowest energy (FM and AFM2 within 1 meV/atom).
[b] NM and in-AFM1 spin configurations are degenerate and of lowest energy.
[c] FM spin configuration of lowest energy.
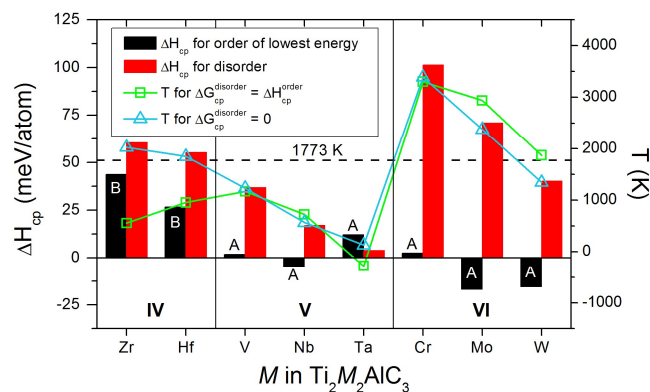
Fig. 4 Formation enthalpy ΔH_{cp} for Ti₂M₂AlC₃, for the ordered structure of lowest energy (black bar) and the disordered structure (red bar), together with the estimated temperature for which the disordered structure is stabilized, $T_{\Delta G=0}$ (open triangles), and the temperature above which the disordered structure is energetically favourable compared to the ordered one, $T_{disorder}$ (open squares).

Table 5 summarizes the results of our phase stability predictions for chemically ordered and disordered (Ti,M)$_{n+1}$AlC$_n$ phases, and can serve as a guide for experimental realization of known as well as new quaternary MAX phase alloys. The first column of phases displays ordered phases predicted to be stable at 0 K, i.e., $\Delta H_{cp}^{order} < 0$. These are expected to be possible to realize experimentally, with either a chemically ordered or disordered distribution of Ti and M. Since synthesis is performed at elevated temperatures, a disordered structure may be energetically preferred over an ordered phase when $T_{disorder} < 1773$ K, as shown in the second column of phases. It should be emphasized that an ordered phase, even if metastable with respect to a stable disordered structure, may be realized through processes including non-equilibrium conditions, such as thin film growth. There are also phases which are not stable in any form at 0 K, i.e., $\Delta H_{cp} > 0$, that can be stabilized at elevated temperatures and possible to realize in a disordered form, as seen in the third column of phases in Table 5.

Table 5 Summary of known as well as new quaternary (Ti,M)$_{n+1}$AlC$_n$ phases expected to be realized experimentally; those predicted to be stable and ordered at 0 K ($\Delta H_{cp}^{order} < 0$) or moderate temperatures, or those disordered due to $T_{disorder} < 1773$ K, or those disordered ($\Delta H_{cp} > 0$) but stabilized with temperature, $T_{\Delta G=0} < 1773$ K.

| n	$\Delta H_{cp}^{order} < 0$ at 0 K		$\Delta H_{cp}^{order} > 0$ at 0 K
	Stable *ordered* phases	*Order → disorder* for $T_{disorder} < 1773$ K	*Disordered* phases stabilized by temperature
1	TiMAlC (M = V, Nb, Ta)	TiMAlC (M = V, Nb, Ta)	TiMAlC (M = Zr, Hf) TiMAlC (M = Cr, Mo, W)
2	MTi₂AlC₂ (M = Nb, Ta) MTi₂AlC₂ (M = W)	MTi₂AlC₂ (M = Nb, Ta) MTi₂AlC₂ (M = W)	MTi₂AlC₂ (M = Zr, Hf) MTi₂AlC₂ (M = V) MTi₂AlC₂ (M = Cr, Mo)
2	TiM₂AlC₂ (M = V, Nb, Ta) TiM₂AlC₂ (M = Cr, Mo, W)	TiM₂AlC₂ (M = V, Nb, Ta)	TiM₂AlC₂ (M = Zr)
3	Ti₂M₂AlC₃ (M = Nb) Ti₂M₂AlC₃ (M = Mo, W)	Ti₂M₂AlC₃ (M = Nb)	Ti₂M₂AlC₃ (M = V, Ta)

3.2   The origin of layered ordered structures

Evident from Table 5 and Fig. 2 to 4 is that M from group V and VI form layered ordered structures in $(\text{Ti},M)_{n+1}\text{AlC}_n$ for $n \geq 2$ and $T_{\text{disorder}} > 1773$ K. The following section will elaborate on the origin behind the formation of chemical order/disorder in quaternary MAX phase alloys, and hence the discussion will include experimentally known as well as hypothetical MAX phases. It should be stressed that the discussion here focus on stability with respect to order/disorder and possible reasons for such formations, and not on absolute stability, i.e. whether or not a phase is stable with respect to competing phases. First, the atomic stacking of $M_{n+1}\text{AlC}_n$ and its subunit $M\text{C}$ will be explored, followed by analysis of the quaternary $(\text{Ti},M)_{n+1}\text{AlC}_n$ phases.

Atomic stacking of MC

$M_{n+1}X_n$ is a sub unit of the $M_{n+1}AX_n$ phases with an AbC stacking (not to be mixed with the notation for A, B, C, D, E, or F type structures referred to in Fig. 1 to 4 and Table 1 to 4) of M and X atoms, see panel (a) in Fig. S11 to S14. To clearly distinct between different stacking positions used for M, A, and X atoms, the following notation are used: A, B, C for M, A, B, C for A, and a, b, c for X. The AbC stacking of M and X can also be found along the 111 direction of NaCl as seen in Fig. S11(a). NaCl is also the type structure for many MX binaries when M is from group IV and V. However, for group VI, there exists no stable $M\text{C}$ binary with an AbCaBc stacking. Instead, other atomic stackings are preferred, e.g., WC with an Ab stacking.

To investigate the possible influence of M and X stacking on the stability of the $M_{n+1}AX_n$ phases we initially considered six different atomic stackings of the $M\text{C}$ binaries as illustrated in Fig. S11. Shown in Fig. 5 is the formation energy ΔE_{f} for $M\text{C}$, i.e., energy for $M\text{C}$ with respect to the energy of the single elements, with different atomic stacking of M and C. For group IV (M = Ti, Zr, Hf) the AbCaBc-stacking (NaCl) is found with lowest energy whereas the Ab-stacking (WC) is the least stable among those considered. For group V (M = V, Nb, Ta) there are three different stacking of lowest energy depending on the volume; AbCaBc (NaCl), AcBaCaBcAbCb (η-MoC), and AcBaBcAb (γ'-MoC), whereas Ab (WC) and AcAb (δ-NbN) stacking are found with highest energy. The result for group VI (M = Cr, Mo, W) show that the stacking of lowest energy is Ab (WC) while the least stable is AbCaBc (NaCl). As an AbCaBc atomic stacking is energetically preferred for M from group IV and V, the corresponding formation of the MAX phases can therefore be expected. Correspondingly, as group VI does not energetically favour AbCaBc-stacking, there is no energy gain in crystallizing
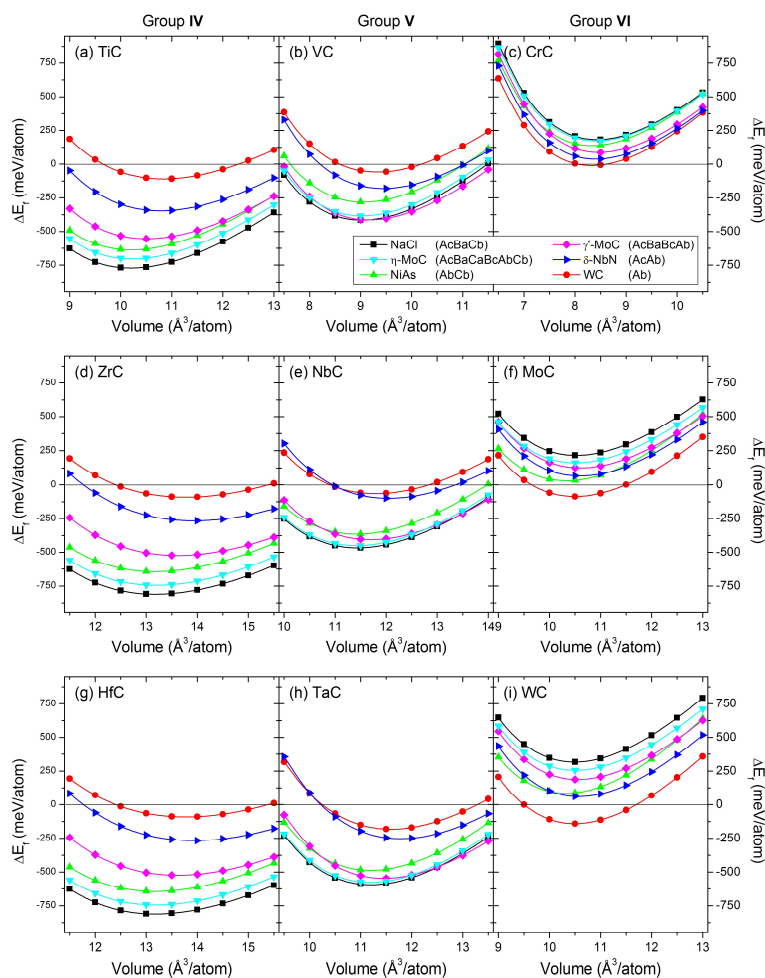
Fig. 5 Formation energy ΔE_{f} for six different atomic stacking sequences of $M\text{C}$ where M = Ti, Zr, Hf, V, Nb, Ta, Cr, Mo, and W.

into the MAX phase structure. In the literature we do find MAX phases from all three groups, but only group IV and V form $M_{n+1}AlC_n$ phases with $n \geq 2$.
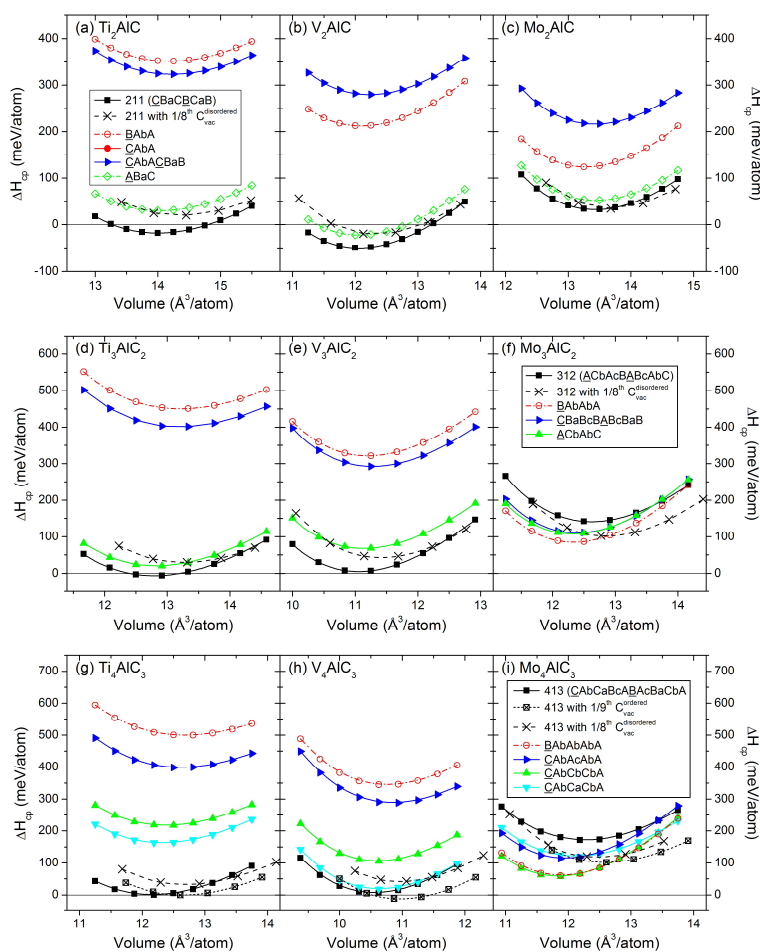
Atomic stacking of $M_{n+1}AlC_n$

We have also considered different atomic stacking of M, Al, and C in $M_{n+1}AlC_n$, as illustrated in Fig. S12 to S14. When the stacking of element A is varied for a fixed atomic stacking of M and X, there is no significant change in energy, while the energy is more sensitive to different stacking of M and X. The results are similar within a group, and for brevity, Ti, V, and Mo are chosen as representatives of M from group IV, V, and VI, respectively. The choice is based upon already synthesized MAX phases within two of these systems, i.e., for M equal to Ti and V.

Fig. 6 shows the formation enthalpy ΔH_{cp} for selected atomic stacking of $M_{n+1}AlC_n$ ($n = 1 - 3$) versus volume. See Fig. S5 for all considered stacking sequences. The MAX phase structure (black filled squares) is stable for all n for Ti and V, but only for $n = 1$ for Mo. Instead, for $n \geq 2$, the Ab stacking of M and X ($n = 2$ and 3) or the AbCbCbA stacking of M and X ($n = 3$), see Fig. S13 and S14, respectively, are of lowest energy with the common feature of having C atoms directly on top of each other. The MAX phase stacking is the least stable for $n \geq 2$, and energetically, the difference between Ab and MAX phase

stacking is 60 and 111 meV/atom for $n = 2$ and 3, respectively. However, even though the non-MAX phase stackings are of lowest energy for Mo and $n \geq 2$, none are predicted stable since $\Delta H_{cp} > 0$.

For $Mo_{n+1}AlC_n$ the MAX phase stacking sequence of carbon is energetically expensive. One way to bypass this is by formation of carbon vacancies. We have modelled this for $n = 1 - 3$ using a disordered distribution of 12.5 % carbon vacancies ($C_{vac}^{disorder}$). For $n = 3$, an ordered distribution of 11 % vacancies (C_{vac}^{order}) was also taken into consideration where every 3rd carbon atom at the Wyckoff 2a-site is replaced by a vacancy.[45, 46] For M = Mo, $C_{vac}^{disorder}$ results in a stabilization for $n = 2$ and 3, though with no effect for $n = 1$. However, ΔH_{cp} remains positive for all n. Correspondingly, for C_{vac}^{order}, then ΔH_{cp} decreases from +171 to +101 meV/atom. For Ti and V, $C_{vac}^{disorder}$ only results in an increased energy, whereas formation of C_{vac}^{order} is preferred for V, with a decrease of ΔH_{cp} from +12 to -12 meV/atom. These results suggest that formation of carbon vacancies can be used as one possible route to lower the energy of the system, and hence possibly increase the phase stability. For Mo-based phases any C site is beneficial, whereas the Wyckoff 2a-site is preferred for V_4AlC_3. This has recently been theoretically and experimentally demonstrated also for Nb_4AlC_3.[46]
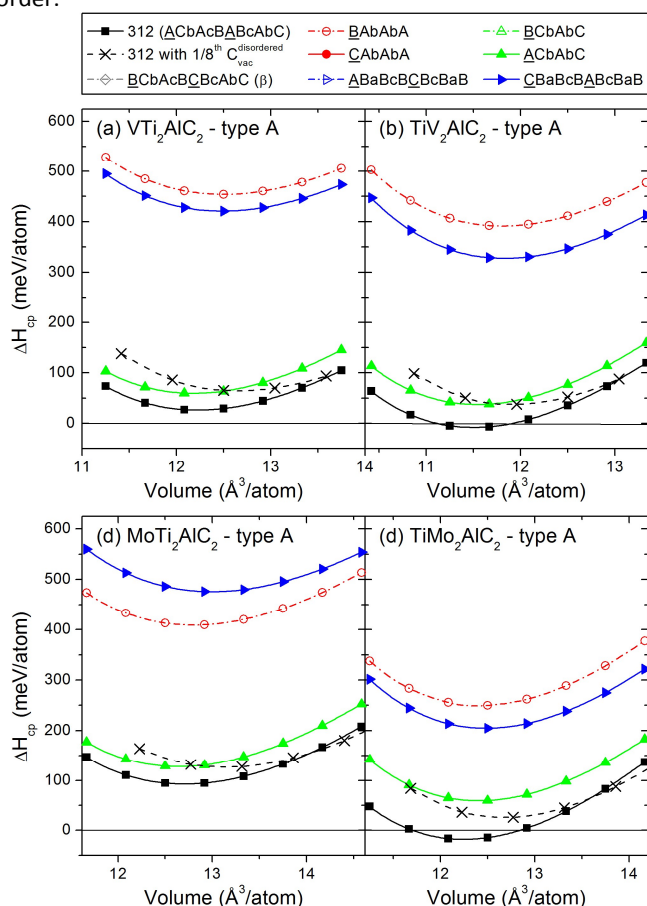

Fig. 6 Formation enthalpy ΔH_{cp} for selected atomic stacking sequences of $M_{n+1}AlC_n$ ($n = 1 - 3$) where M = Ti, V, and Mo. For the MAX phase stacking (black symbols), disordered and ordered carbon vacancies have also been modelled for $n = 1 - 3$ and $n = 3$, respectively.

Atomic stacking of quaternary ordered MAX phases

The formation enthalpy ΔH_{cp} for ordered layers of type A of MTi$_2$AlC$_2$ and TiM_2AlC$_2$ with different stacking sequences and configurations including carbon vacancies is shown in Fig. 7, where V and Mo are again chosen as representatives of M from group V and VI, respectively. VTi$_2$AlC$_2$, TiV$_2$AlC$_2$, MoTi$_2$AlC$_2$, and TiMo$_2$AlC$_2$ are all of type A layering, with the MAX phase stacking being of lowest energy. Comparing to Mo$_3$AlC$_2$ where an AbAbA stacking of Mo and C is preferred, see Fig. 6(f), the substitution of Mo with Ti on the Wyckoff 2a-site to form TiMo$_2$AlC$_2$ (type A) apparently change the energetically preferred stacking.

The corresponding calculations have also been performed for Ti$_2M_2$AlC$_3$, see Fig. 8, and the change in preferred stacking is evident also for Ti$_2$Mo$_2$AlC$_3$ (type A) as shown in Fig. 8(d), in comparison with Mo$_4$AlC$_3$ as shown in Fig. 6(i). However, for Ti$_2$Mo$_2$AlC$_3$ (type B) in Fig. 8(c), see schematic in Fig 1, the MAX phase stacking is not of lowest energy. Also notice that an ordered configuration of carbon vacancies is found to promote a decrease in ΔH_{cp} for both Ti$_2$V$_2$AlC$_3$ and Ti$_2$Mo$_2$AlC$_3$ of type B order.

Fig. 7 Formation enthalpy ΔH_{cp} for selected atomic stacking sequences of ordered (a) VTi$_2$AlC2, (b) TiV2AlC2, (c) MoTi2AlC2, and (d) TiMo2AlC2, with type A layering. For the MAX phase stacking, disordered carbon vacancies have also been considered ($\times$).
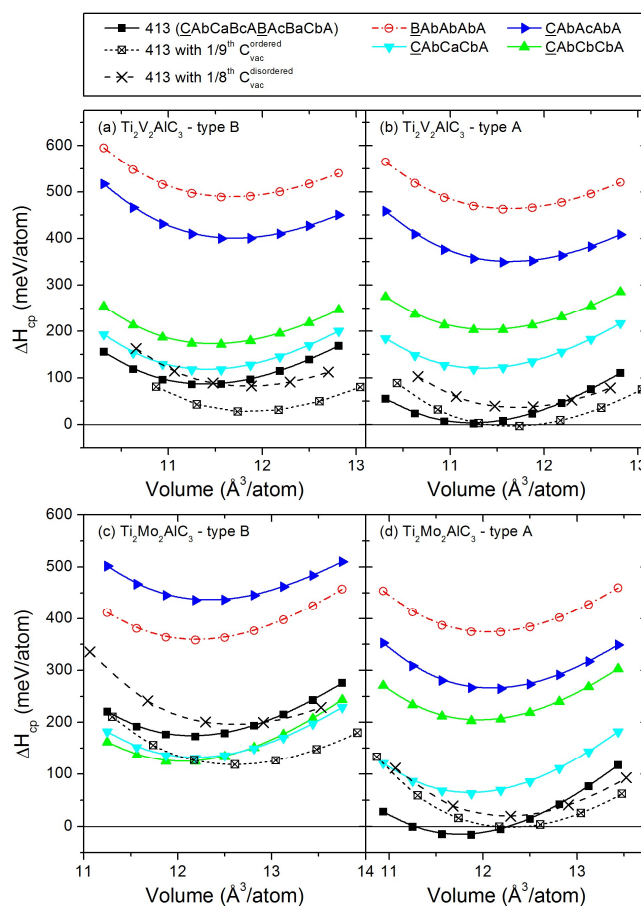
Fig. 8 Formation enthalpy ΔH_{cp} for selected atomic stacking sequences of ordered Ti$_2$V$_2$AlC$_3$ of (a) type B and (b) type A, and Ti$_2$Mo$_2$AlC$_3$ of (c) type B and (d) type A. For the MAX phase stacking, disordered ($\times$) and ordered ($\square$) carbon vacancies have also been considered

Our results for MoC, ordered TiMo$_2$AlC$_2$ and Ti$_2$Mo$_2$AlC$_3$ (the latter two of type A layering), supports the assumption made by Babak et $al.$[24] that having Mo atoms surrounded by C in a face-centred configuration is energetically unfavourable. However, the assumption made is not valid for the AbAbAbA stacking of type B layered Ti$_2$Mo$_2$AlC$_3$, red circles in Fig. 8(c), which is rather high in energy even though the atomic stacking of Mo and C is of the same kind as for low energy WC type-structure of MoC as seen in Fig. 5(f). Hence, having Mo atoms surrounded by C in a face-centred configuration may be energetically unfavourable, but it cannot fully explain why, e.g., the calculated formation enthalpy of TiMo$_2$AlC$_2$ (type A) is very low (ΔH_{cp} = -18 meV/atom) compared to Ti$_3$AlC$_2$, (ΔH_{cp} = -6 meV/atom) and Mo$_3$AlC$_2$ with either MAX phase stacking (ΔH_{cp} = +141 meV/atom) or AbAbA stacking (ΔH_{cp} = +85 meV/atom). In other words, formation of ordered TiMo$_2$AlC$_2$ (type A) cannot simply be explained by breaking the unfavourable ABC-stacking of Mo and C in Mo$_3$AlC$_2$ by substituting Mo at Wyckoff position 2a with Ti. The same argument can also be made for Ti$_2$Mo$_2$AlC$_3$.

The origin may, at least in part, be the different electronegativity of Ti (1.54) and Mo (2.16) as seen in Fig. 9(a). We have therefore performed Bader analysis to obtain the charge of each atom in M_3AlC$_2$, TiM_2AlC$_2$ (type A), M_4AlC$_3$, and Ti$_2M_2$AlC$_2$ (type A), for M = Zr, Hf, V, Nb, Ta, Cr, Mo, W. Fig. 9(b-e) shows the atomic Bader charge of M, Al, and C. The overall

trend is that the highly electronegative C is always negatively charged, i.e. with a surplus of electrons, M is positively charged, i.e. electron deficient, with M at Wyckoff 2a-site in 312 or M at Wyckoff 4f-site in 413 phases being more positive than M at Wyckoff 4f-site in 312 or M at Wyckoff 4e-site in 413. This can be related to the carbon layers on both sides of M at 2a- or 4f-site in 312 or 413, respectively. Al, on the other hand, is negatively charged for phases with M from group IV, close to neutral when M is from group V, and positive when M is from group VI.

These trends can be correlated to the different electronegativity's of M as shown in Fig. 9(a), where M from group IV (Ti, Zr, Hf) is less electronegative than Al, M from Group V (Nb, Ta, V) is close to or less electronegative than Al, and M from group VI (Cr, Mo, W) are all more electronegative than Al.

To investigate how fewer electrons at and close to Al may have an influence on the low energy of layered ordered structures with M from group VI, the electronic structure and chemical bonding was evaluated. The total and atomic density of states (DOS) of Ti$_3$AlC$_2$ M_3AlC$_2$ and TiM_2AlC$_2$ (type A), with M = V and Mo, are shown in Fig. 10(a – e), where the vertical line indicates the Fermi level E_f. Overall, the presented DOS can be divided into several parts; (i) the peak at low energies, from -14 to -9 eV, can mainly be attributed to localized C-s electrons, (ii) between -9 and -6 eV, localized Al-s states dominate, (iii) the bonding states of M-d and C-p are found between -6 and -2 eV, (iv) from -4 and up to E_f, the bonding states of M(4f)-d and Al-p electrons can be found , and (v) the states at E_f originate primarily from M-d, and in particular from M(4f). From the DOS curves in panel (a) and (c), it is clear that Ti$_3$AlC$_2$ and V$_3$AlC$_2$ have close resemblance, though the states of the latter is shifted down in energy due to the extra electron of V. Both are found

with the Fermi level E_f located in a valley, indicating that the bonding valence bands are completely filled. Going to Mo$_3$AlC$_2$ in panel (e), the bonding peaks of M-d, Al-p, and C-p are shifted towards lower energy due to an increased number of valence electrons. E_f is no longer located in a local minima, and is instead found in a region implying occupation of anti-bonding states, consistent with a predicted reduced stability evident from ΔH_{cp} = -6, +5, and +141 meV/atom for M = Zr, Nb, and Mo in M_3AlC$_2$, respectively. For TiV$_2$AlC$_2$, the DOS is not affected much as compared to Ti$_3$AlC$_2$ and V$_3$AlC$_2$. However, when Mo(2a) is substituted with Ti in Mo$_3$AlC$_2$, the number of states at E_f is reduced by almost 50%, and C-s and bonding states of M-d and C-p are shifted to lower energies. Compared to Ti$_3$AlC$_2$, the bonding states of M(4f)-d and Al-p in TiMo$_2$AlC$_2$ are found at lower energies. This results are an indication of the reduced total energy for type A layering of the TiMo$_2$AlC$_2$ phase as compared to Ti$_3$AlC$_2$ and Mo$_3$AlC$_2$.

Bonding analysis in terms of the projected crystal orbital Hamiltonian population (pCOHP) have been performed for nine interactions in M_3AlC$_2$ and TiM_2AlC$_2$ (type A layering) for M = V and Mo, see schematic in Fig. 10. In order to facilitate interpretation and to preserve the analogy to crystal orbital overlap population (COOP) analysis, results are here presented as –pCOHP, rather than pCOHP. From the pCOHP curves in Fig. 10 it is clear that the nearest neighbor interactions of M(2a)-C, M(4f), and M(4f)-Al are typically optimized for M_3AlC$_2$ and TiM_2AlC$_2$, with bonding orbitals completely filled and antibonding orbitals empty below E_f. The only exception is for M(4f)-C, for M = V and Mo, which displays a small antibonding contribution close to E_f. M(2a)-M(2a) and M(4f)-M(4f) in-plane interactions all have bonding orbitals completely filled and
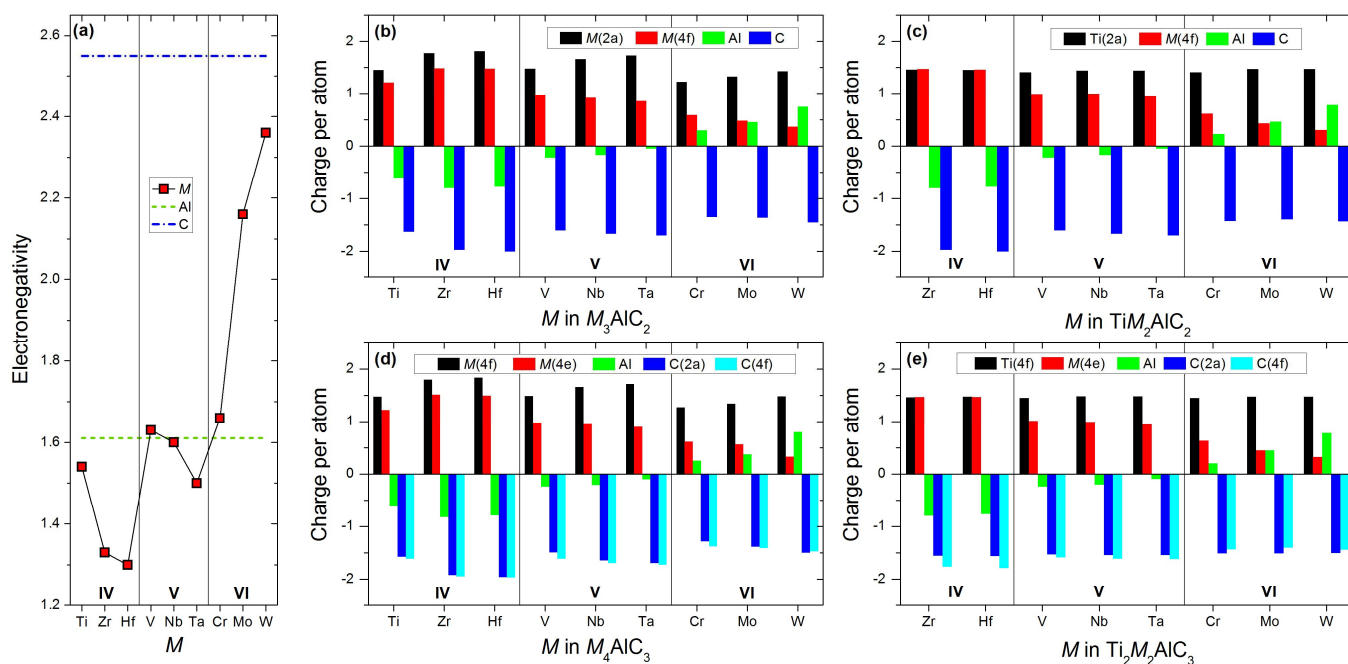
Fig. 9 (a) Electronegativity of M, Al, and C. Charge per atom for (b) M_3AlC$_2$, (c) TiM_2AlC$_2$ of type A, (d) M_4AlC$_3$, and (e) Ti$_2M_2$AlC$_3$ of type A
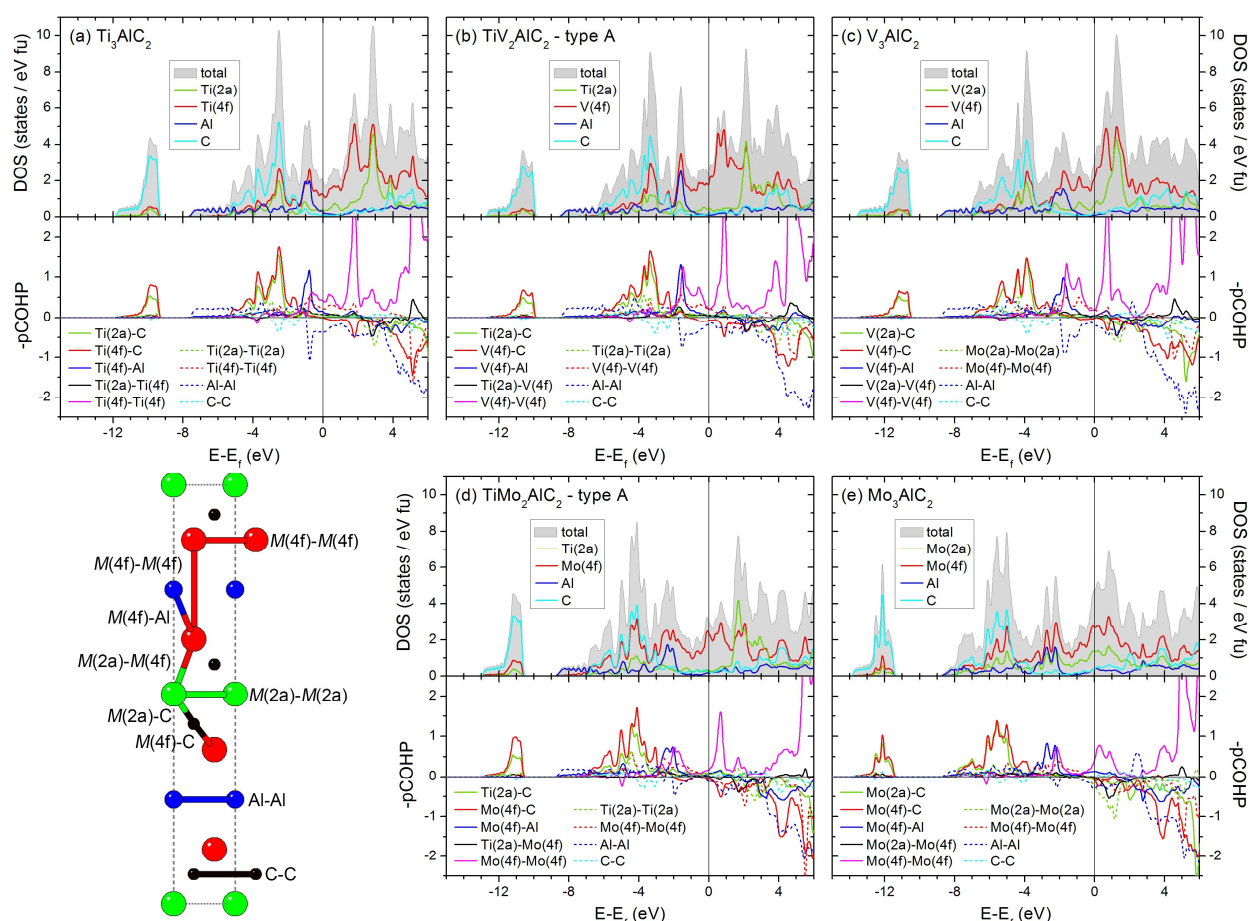
Fig. 10 Calculated total and atomic density of states (DOS) and projected crystal overlap Hamiltonian population (pCOHP) analysis for (a) Ti$_3$AlC$_2$, (b) TiV$_2$AlC$_2$ (type A), (c) V$_3$AlC$_2$, (d) TiMo$_2$AlC$_2$ (type A), and (e) Mo$_3$AlC$_2$. The schematic five out-of-plane and four in-plane pCOHP interactions are shown at the bottom of panel (a) – (e) with solid and dashed lines, respectively.

antibonding orbitals empty below E_f. For M = Ti and V, C-C and especially Al-Al in-plane interactions have filled antibonding states below E$_f$. These are also present for M = Mo but much more reduced. For brevity, pCOHPs of M_4AlC$_3$ and Ti$_2M_2$AlC$_3$ are not shown here, as they show large resemblance with M_3AlC$_2$ and TiM_2AlC$_2$, though the same arguments apply for these phases.

The low energy of ordered TiM_2AlC$_2$ (type A) with M from group VI, can thus be related to; (i) M atoms surrounded by C in a face-centered configuration is energetically unfavourable and substitution of M(2a) with Ti breaks this stacking, (ii) as M have a higher electronegativity compared to Al, the Al becomes more positively charged which results in fewer electrons available for populating the antibonding Al-Al interaction (which would increase the energy of the system), and (iii) bonding states are shifted to lower energies as compared to Ti$_3$AlC$_2$ without populating antibonding states, thus lowering the total energy of the system. Corresponding analysis of Ti$_2M_2$AlC$_3$ (M = Cr, Mo, W) reveals similar results and supports the statements above.

3.3 Off-stoichiometry in ordered M'$_{3-m}$M$_m$AlC$_2$

Experimental evidence for TiCr$_2$AlC$_2$ has been reported, with 100 at% Ti at Wyckoff 2a and 100 at% Cr at Wyckoff 4f,[22, 23] whereas off-stoichiometric quaternary phases have been reported for Ti$_{1.5}$Mo$_{1.5}$AlC$_2$ and V$_{1.5}$Cr$_{1.5}$AlC$_2$,[12, 24] with 100 at%

Ti or V at Wyckoff 2a and 75 at% Mo or Cr at Wyckoff 4f (25 at% Ti or V). These results raise the question how much it is possible to deviate from the TiM_2AlC$_2$ composition while still retaining an ordered, or a semi-ordered, structure with one of the Wyckoff sites (2a or 4f) occupied by only one element.

To model this we constructed SQS supercells with a disordered distribution of M atoms on one of the M sites only. Fig. 11 shows the formation enthalpy ΔH_{cp} at 0 K (solid symbols and solid lines) and Gibbs free energy ΔG_{cp} at 1773 K (open symbols and dashed lines) as function m in $M'_{3-m}M_m$AlC$_2$ where M' = Ti, V, and M = V, Cr, Mo. For Ti$_{3-m}$V$_m$AlC$_2$ in panel (a), ordered and semi-ordered structures are found with lowest energy at 0 K for all m, whereas a disordered distribution of Ti and V is favoured at 1773 K. For the other three quaternary systems the disordered structure is found at much higher energies and at 1773 K, the ordered and semi-ordered structures are still the preferred ones. For comparison, the composition of synthesized ordered and semi-ordered structures of TiCr$_2$AlC$_2$,[22, 23] V$_{1.5}$Cr$_{1.5}$AlC$_2$,[12] and Ti$_{1.5}$Mo$_{1.5}$AlC$_2$,[24] are marked with a vertical solid line, which is data consistent with here presented calculations. This indicates that ordered layered phases can deviate slightly from "perfect" stoichiometry, i.e., deviate from only one atomic element at Wyckoff 2a (4f for Ti$_2M_2$AlC$_3$) and/or 4f (4e for Ti$_2M_2$AlC$_3$), while still being stable. This may explain reported compositional

ARTICLE
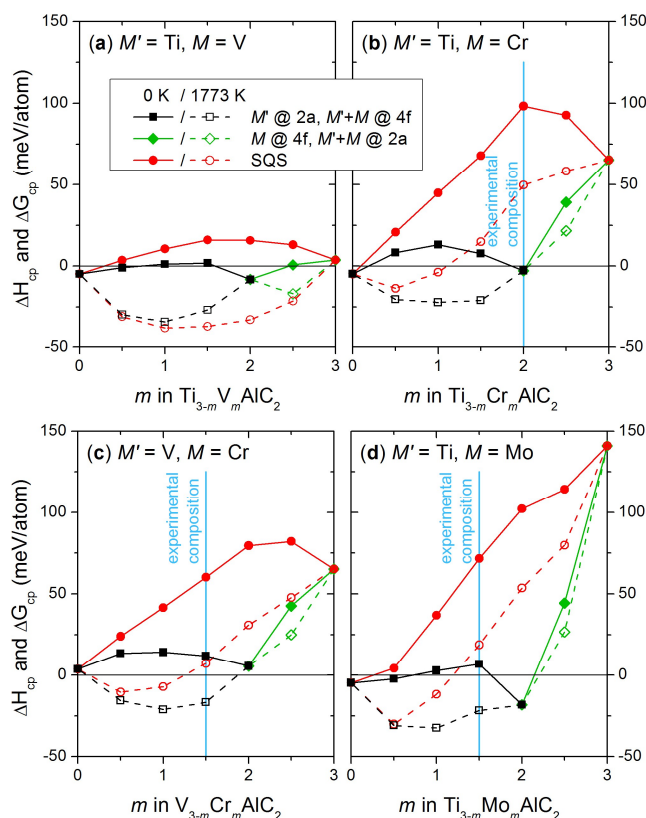
Fig. 11 Formation enthalpy ΔH_{cp} at 0 K (solid symbols and solid lines) and Gibbs free energy ΔG_{cp} at 1773 K (open symbols and dashed lines) for $M'_{3-m}M_mAlC_2$ where M' = Ti, V, and M = V, Cr, Mo, for semi-ordered layered structures and solid solutions (SQS). The vertical solid line represents experimentally obtained ordered or semi-ordered structures.

deviations from TiM_2AlC_2 and $Ti_2M_2AlC_3$ for $V_{1.5}Cr_{1.5}AlC_2$ [12], $V_{2.2}Cr_{1.8}AlC_3$,[12] $Ti_{1.5}Mo_{1.5}AlC_2$,[24] $Ti_{2.2}Mo_{1.8}AlC_3$,[24] and $Ti_{1.5}Cr_{2.5}AlC_3$.[23] Caspi *et al*.[12] showed that in $V_{2.2}Cr_{1.8}AlC_3$ there was mixture of V and Cr with different concentrations at Wyckoff 4f (80 at% V and 20 at% Cr) and 4e (30 at% V and 70 at% Cr).

The recently discovered $TiCr_2AlC_2$, $Ti_{1.5}Mo_{1.5}AlC_2$, $Ti_2Mo_2AlC_3$, $V_{1.5}Cr_{1.5}AlC_2$, and here predicted stable phases of novel TiM_2AlC_2 and $Ti_2M_2AlC_3$ compositions, belong to a new family of chemically ordered quaternary MAX phases. These phases allow inclusion of elements in combinations previously not forming MAX phases, e.g., to date there are no $Mo_{n+1}AlC_n$ phases reported. These novel combinations can then be used to alter or add new properties to this family of laminated materials. This was demonstrated by Babak *et al*.[24], showing that bulk, shear, and elastic moduli of $TiMo_2AlC_2$ and $Ti_2Mo_2AlC_3$ were improved compared to the pure ternaries. Furthermore, Al is the A-group element in all realized ordered MAX phases to date,[12, 22-25] and it is also an element which can be readily etched in HF to form MXene.[26] Recently, new ordered MXenes ($TiMo_2C_2$, $Ti_2Mo_2C_3$, $TiCr_2C_2$) were synthesized from ordered quaternary MAX phases, and even more hypothetical MXenes were theoretically suggested [28]. Still, an important aspect missing in the prediction of new MXenes is the evaluation of the parent material, which is the MAX phase. Reliable calculations for prediction of stability of new materials should include all competing phases in the system and not focus only on the energy of a phase with respect to its constituent atoms, as demonstrated in Ref. [38].

4 Conclusions

We have performed a systematic theoretical study of phase stability of chemically ordered and disordered quaternary $(Ti,M)_{n+1}AlC_n$ ($n = 1 - 3$) phases, where M = Zr, Hf (group IV), M = V, Ta, Nb (group V), and M = Cr, Mo, W (group VI). At 0 K, we predict layered ordered structures to be stable for M from group V and VI. Out of these, only TiM_2AlC_2 (M = Cr, Mo, W) and $Ti_2M_2AlC_2$ (M = Mo, W) are identified with an order-disorder temperature $T_{disorder} > 1773$ K (typical bulk synthesis temperature) and hence likely to be chemically ordered if synthesized, while the others are found with $T_{disorder} < 1773$ K and therefore expected to have a chemically disordered distribution of Ti and M. It should be emphasized that a metastable ordered phase may very well be realized at non-equilibrium conditions through e.g. thin film deposition. Phases predicted to not be stable at 0 K can be stabilized at elevated temperatures in a chemically disordered form, being the case for group IV and MTi_2AlC_2 (M = V, Cr, Mo), and $Ti_2M_2AlC_3$ (M = V, Ta). These results are in accordance with experimental findings of disordered $(Ti_{0.5}V_{0.5})_2AlC$, $(Ti_{0.5}Nb_{0.5})_2AlC$, and $(Ti_{0.4}Ta_{0.6})_2AlC$, $(V_{0.5}Ti_{0.5})_3AlC_2$ and ordered $TiCr_2AlC_2$, $TiMo_2AlC_2$, $Ti_2Mo_2AlC_3$. In addition to the here predicted stable disordered alloys, the predicted stable ordered $Ti_2W_2AlC_2$ and close to stable ordered $Ti_2Cr_2AlC_3$ is yet to be experimentally verified. The driving force for the formation and stability of these layered and chemically ordered structures, with M from group V and VI, is at least in part explained by; (i) M surrounded by C in a face-centred configuration is energetically unfavourable when M is from group VI, and this is changed by substitution with Ti, and (ii) M from group VI have a larger electronegativity than Al, and thus fewer electrons will be available for populating antibonding Al-Al orbitals. Adding a fourth element to form ordered quaternary MAX phases allows for new novel elemental combinations which can be used to add/tune new properties in this family of atomic laminates.

Acknowledgements

ARTICLE

References

1. P. Eklund, M. Beckers, U. Jansson, H. Högberg and L. Hultman, *Thin Solid Films*, 2010, **518**, 1851-1878.
2. M. W. Barsoum and T. El-Raghy, *Am. Scientist*, 2001, **89**, 334-343.
3. A. S. Ingason, A. Mockute, M. Dahlqvist, F. Magnus, S. Olafsson, U. B. Arnalds, B. Alling, I. A. Abrikosov, B. Hjörvarsson, P. O. Å. Persson and J. Rosen, *Phys. Rev. Lett.*, 2013, **110**, 195502.
4. R. Meshkian, A. S. Ingason, U. B. Arnalds, F. Magnus, J. Lu and J. Rosen, *APL Materials*, 2015, **3**, 076102.
5. P. Eklund, M. Dahlqvist, O. Tengstrand, L. Hultman, J. Lu, N. Nedfors, U. Jansson and J. Rosén, *Phys. Rev. Lett.*, 2012, **109**, 035502.
6. A. S. Ingason, A. Petruhins, M. Dahlqvist, F. Magnus, A. Mockute, B. Alling, L. Hultman, I. A. Abrikosov, P. O. Å. Persson and J. Rosen, *Mater. Res. Lett.*, 2014, **2**, 89-93.
7. M. Dahlqvist, A. S. Ingason, B. Alling, F. Magnus, A. Thore, A. Petruhins, A. Mockute, U. B. Arnalds, M. H. Sahlberg, B. Hjörvarsson, I. A. Abrikosov and J. Rosen, *submitted*, 2015.
8. J. C. Schuster, H. Nowotny and C. Vaccaro, *J. Solid State Chem.*, 1980, **32**, 213-219.
9. H. Nowotny, P. Rogl and J. C. Schuster, *J. Solid State Chem.*, 1982, **44**, 126-133.
10. M. W. Barsoum, I. Salama, T. El-Raghy, J. Golczewski, H. J. Seifert, F. Aldinger, W. D. Porter and H. Wang, *Metall. Mater. Trans. A*, 2002, **33**, 2775-2779.
11. C. L. Yeh and W. J. Yang, *Ceram. Int.*, 2013, **39**, 7537-7544.
12. E. a. N. Caspi, P. Chartier, F. Porcher, F. Damay and T. Cabioc'h, *Mater. Res. Lett.*, 2015, **3**, 100-106.
13. S. Lin, P. Tong, B. S. Wang, Y. N. Huang, W. J. Lu, D. F. Shao, B. C. Zhao, W. H. Song and Y. P. Sun, *J. Appl. Phys.*, 2013, **113**, 053502 053501-053506.
14. A. Mockute, M. Dahlqvist, J. Emmerlich, L. Hultman, J. M. Schneider, P. O. Å. Persson and J. Rosen, *Phys. Rev. B*, 2013, **87**, 094113.
15. Z. Liu, T. Waki, Y. Tabata and H. Nakamura, *Phys. Rev. B*, 2014, **89**, 054435 054431-054436.
16. A. Mockute, J. Lu, E. J. Moon, M. Yan, B. Anasori, S. J. May, M. W. Barsoum and J. Rosen, *Mater. Res. Lett.*, 2014, **3**, 16-22.
17. Q. Z. Tao, C. F. Hu, S. Lin, H. B. Zhang, F. Z. Li, D. Qu, M. L. Wu, Y. P. Sun, Y. Sakka and M. W. Barsoum, *Mater. Res. Lett.*, 2014, **4**, 192-198.
18. A. Petruhins, A. S. Ingason, J. Lu, F. Magnus, S. Olafsson and J. Rosen, *J. Mater. Sci.*, 2015, **50**, 4495-4502.
19. R. Salikhov, A. S. Semisalova, A. Petruhins, A. S. Ingason, J. Rosen, U. Wiedwald and M. Farle, *Mater. Res. Lett.*, 2015, **3**, 156-160.
20. S. Kerdsongpanya, K. Buchholt, O. Tengstrand, J. Lu, J. Jensen, L. Hultman and P. Eklund, *J. Appl. Phys.*, 2011, **110**, 053516.
21. M. Naguib, G. W. Bentzel, J. Shah, J. Halim, E. N. Caspi, J. Lu, L. Hultman and M. W. Barsoum, *Mater. Res. Lett.*, 2014, **2**, 233-240.
22. Z. Liu, E. Wu, J. Wang, Y. Qian, H. Xiang, X. Li, Q. Jin, G. Sun, X. Chen, J. Wang and M. Li, *Acta Mater.*, 2014, **73**, 186-193.
23. Z. Liu, L. Zheng, L. Sun, Y. Qian, J. Wang and M. Li, *J. Am. Ceram. Soc.*, 2014, **97**, 67-69.
24. B. Anasori, M. Dahlqvist, J. Halim, E. J. Moon, J. Lu, B. C. Hosler, C. E. a. N., S. J. May, L. Hultman, P. Eklund, J. Rosén and M. W. Barsoum, *J. Appl. Phys.*, 2015, **118**, 094304.
25. B. Anasori, J. Halim, J. Lu, C. A. Voigt, L. Hultman and M. W. Barsoum, *Scripta Mater.*, 2015, **101**, 5-7.
26. M. Naguib, V. N. Mochalin, M. W. Barsoum and Y. Gogotsi, *Adv. Mater.*, 2014, **26**, 992-1005.
27. R. Meshkian, L.-Å. Näslund, J. Halim, J. Lu, M. W. Barsoum and J. Rosen, *Scripta Mater.*, 2015, **108**, 147-150.
28. B. Anasori, Y. Xie, M. Beidaghi, J. Lu, B. C. Hosler, L. Hultman, P. R. C. Kent, Y. Gogotsi and M. W. Barsoum, *ACS Nano*, 2015, DOI: http://dx.doi.org/10.1021/acsnano.5b03591.
29. P. E. Blöchl, *Phys. Rev. B*, 1994, **50**, 17953-17979.
30. G. Kresse and D. Joubert, *Phys. Rev. B*, 1999, **59**, 1758-1775.
31. G. Kresse and J. Hafner, *Phys. Rev. B*, 1993, **47**, 558-561.
32. G. Kresse and J. Furthmüller, *Comput. Mater. Sci.*, 1996, **6**, 15-50.
33. G. Kresse and J. Furthmüller, *Phys. Rev. B*, 1996, **54**, 11169-11186.
34. J. P. Perdew, K. Burke and M. Ernzerhof, *Phys. Rev. Lett.*, 1996, **77**, 3865-3868.
35. H. J. Monkhorst and J. D. Pack, *Phys. Rev. B*, 1976, **13**, 5188-5192.
36. A. Zunger, S. H. Wei, L. G. Ferreira and J. E. Bernard, *Phys. Rev. Lett.*, 1990, **65**, 353-356.
37. M. Dahlqvist, B. Alling, I. A. Abrikosov and J. Rosén, *Phys. Rev. B*, 2010, **81**, 024111.
38. M. Dahlqvist, B. Alling and J. Rosén, *Phys. Rev. B*, 2010, **81**, 220102.
39. A. Mockute, P. O. Å. Persson, F. Magnus, A. S. Ingason, S. Olafsson, L. Hultman and J. Rosen, *Phys. Status Solidi Rapid Res. Lett.*, 2014, **8**, 420-423.
40. S. Maintz, V. L. Deringer, A. L. Tchougréeff and R. Dronskowski, *Journal of Computational Chemistry*, 2013, **34**, 2557-2567.
41. V. L. Deringer, A. L. Tchougréeff and R. Dronskowski, *The Journal of Physical Chemistry A*, 2011, **115**, 5461-5466.
42. R. Dronskowski and P. E. Bloechl, *The Journal of Physical Chemistry*, 1993, **97**, 8617-8624.
43. V. Presser, M. Naguib, L. Chaput, A. Togo, G. Hug and M. W. Barsoum, *Journal of Raman Spectroscopy*, 2012, **43**, 168-172.
44. I. Salama, T. El-Raghy and M. W. Barsoum, *J. Alloys Compd.*, 2002, **347**, 271-278.
45. J. Etzkorn, M. Ade and H. Hillebrecht, *Inorg. Chem.*, 2007, **46**, 7646-7653.
46. H. Zhang, T. Hu, X. Wang, Z. Li, M. Hu, E. Wu and Y. Zhou, *Scientific Reports*, 2015, **5**, 14192.